# Deliverable

## H2020 COMPET-05-2015 project
## "Small Bodies: Near And Far (SBNAF)"

**Topic**: COMPET-05-2015 - Scientific exploitation of astrophysics, comets, and planetary data

**Project Title**: Small Bodies Near and Far (SBNAF)

**Proposal No**: 687378 - SBNAF - RIA

**Duration**: Apr 1, 2016 - Mar 31, 2019

| | |
|---|---|
| **WP** | **WP6, Synergies from ground and space** |
| **Del.No** | **D6.5** |
| **Title** | **"Ground truth" shape models** |
| **Lead Beneficiary** | UAM |
| **Nature** | Report |
| **Dissemination Level** | Public |
| **Est. Del. Date** | 31 March 2017 |
| **Version** | 1.0 |
| **Date** | September 29, 2017 |
| **Lead Author** | Alí-Lagoa, V.; MPE (vali@mpe.mpg.de) |

Objectives of WP: To combine observational data from space and ground, from remote, disk-integrated data and disk-resolved data from interplanetary missions to obtain (validated) high-quality model solutions for a wide range of applications: improvement of the scientific understanding, answering key questions for the reconstruction of minor body properties, calibration aspects, support for Gaia density determination, Hayabusa-2 target characterization and operational support, tools and methods for applications to large object samples.

# Description of deliverable

Shape models from both convex and non-convex inversion vs. ground truth.

# Contents



# 1 Introduction and scope

In this deliverable we summarise SBNAF works aimed at obtaining non-convex shapes of asteroids that have been published or accepted for publication in peer-reviewed journals. One article of particular relevance to the SBNAF Milestone 2, Bartczak & Dudziński, has been accepted for publication in Monthly Notices of the Royal Astronomical Society in September 2017. It is based on SAGE, a lightcurve inversion algorithm that produces non-convex shapes based on genetic evolution.

The optimal way to validate shape models (whether convex or non-convex), periods, spin axis orientations, and the scaling of said shapes derived from light curve inversion (LCI) methods is to compare them with "ground-truth" information. The difficulty for small bodies is that ground truth is very scarce as most of them cannot be resolved remotely. In this deliverable we also evaluate how much ground truth information there is available for objects observed from space craft in order to optimally select good science and benchmark cases for future work. Further benchmarking against thermal data –also sensitive to the shape and rotational properties– has been programmed for deliverables D6.6 and D6.7.

Because of the scarcity of spacecraft data and in spite of a number of limitations, we also consider high-quality occultation chords (see D6.1 for brief introductory notes) and adaptive optics (AO) images as useful "ground truth" against which to test LCI shape models. Although AO data requires model-dependent assumptions, their increasing availability for small bodies suggests they are an important source of shape information (see e.g. Marchis et al. 2006; Descamps et al. 2011; Carry et al. 2012; Hanuš et al. 2017). Specifically, an ESO large programme has been recently awarded to a team led by P. Vernazza (LAM) to survey a set of 40 large main belt asteroids with VLT/SPHERE. Some of our team members are collaborators in said project, which offers great prospects for SBNAF given the high degree of overlap in our list of targets. Namely, about half of the ESO large programme's sample are either part of our "Gaia perturbers" sample and/or potential secondary calibrators (see deliverable D4.6).

In this context, and considering the ultimate goal of confronting convex and non-convex shape models with ground truth, our aims in this document are

- to provide some comments and references on AO data (Sec. 2) and the techniques employed to derive convex and non-convex shapes from LCI (Sec. 3). More introductory information on these topics and further references are available in our public website[1].
- to present the shape models derived by Bartczak & Dudziński (accepted) with the SAGE algorithm and validated against the ground truth: spacecraft-based shape of (433) Eros (Sec. 4.1), and a rich set of occultation chords available for (9) Metis (Sec. 4.2).
- to summarise other SBNAF works (or with participation of SBNAF members) where non-convex shapes are determined: Marsset et al. (2017) in Sec. 4.3, and Marciniak et al. (accepted, see D6.6) in Secs. 4.4.
- to collect available ground truth information about small bodies based on spacecraft (Table 3), occultations, and AO data that will guarantee the derivation of non-convex shape models using the SAGE algorithm in forthcoming SBNAF work (Secs. 5.1–5.2), including convex and non-convex shape models, depending on availability.
- to collect shape-related information for a set of targets and evaluate whether they are compelling candidates for future work (Sec. 6). Some of these targets could be finally selected as adequate secondary calibrators; in other cases, more ground truth is foreseen to be available, such as the Hayabusa-2 target (101955) Bennu. This will also be a valuable reference to help plan further data acquisition within our project.

## 2 Disc-resolved images from adaptive optics (AO)

Their sizes and locations in the solar system make most small bodies impossible to resolve from Earth. The limiting effects of diffraction and the atmosphere blur and smear the images so that they are not distinguishable from (idealised) point-like sources (see Fig. 1, left panel). Although diffraction can be mitigated by building bigger and bigger telescopes (Fig. 1, right panel), the atmosphere introduces a minimum amount of "blurring", called *seeing*. This affects all telescopes, regardless of their size, which poses a difficulty for small body studies because the angular sizes of the vast majority of these objects is smaller than the seeing disc.

Adaptive optics is a technique whereby this limitation is overcome to some extent. In a nutshell, an extremely fast system (a wavefront sensor) is used to record and characterise the distortions suffered by an artificial point source (typically created with powerful lasers) in real time. With a fast electromechanical system, a deformable mirror is acted upon and deformed to correct for the distortion taking into account the information obtained by the wavefront sensor. Examples of AO images of asteroid (216) Kleopatra are shown in Fig. 2 next to renderings of the corresponding shape model obtained by Descamps et al. (2011).

The AO images of Fig. 2 have two silhouettes superimposed. These correspond to the shape model shown to the right of the AO images scaled with two independent size estimates, one based on the radiometric equivalent diameter (see e.g. deliverable D6.1, Sec. 2.2), the other one on radar data (Descamps et al. see the references in 2011). These silhouettes show that the reconstructed

[1] `http://www.mpe.mpg.de/~tmueller/sbnaf/techniques.html`.

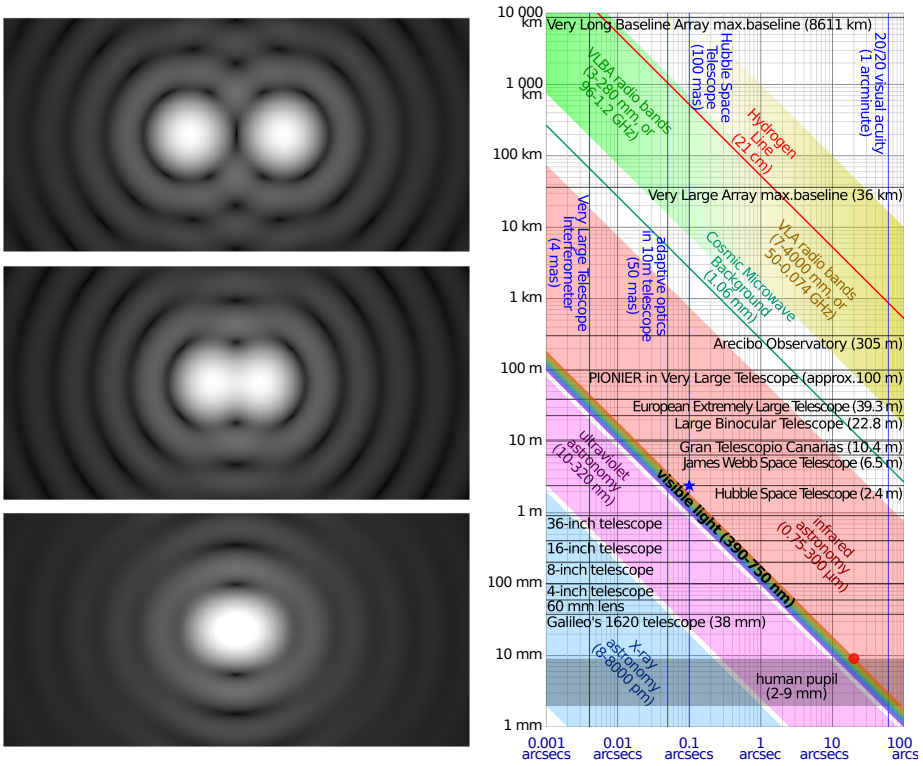


Figure 1: Left: Diffraction patterns of two point sources observed through a circular aperture. These are called Airy discs. Credit: By Spencer Bliven - Own work, Public Domain, https://commons.wikimedia.org/w/index.php?curid=31456019. Right panel: apperture versus diffraction limit for different wavelengths. Relevant astronomical instruments as well as the human eye (red circle on the lower right) are included. Credit: By Cmglee - Own work, CC BY-SA 3.0, https://commons.wikimedia.org/w/index.php?curid=19129100.

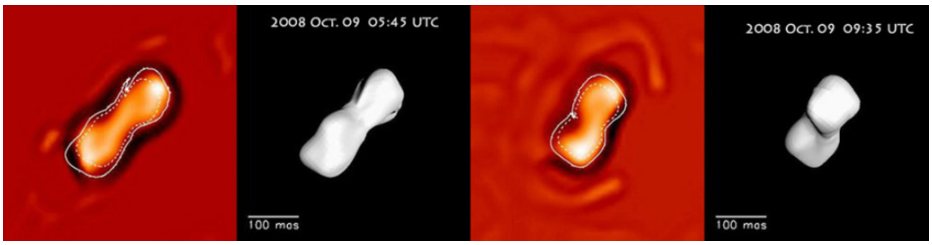


Figure 2: Subsample of AO images of asteroid (216) Kleopatra and the corresponding shape model (black background) taken from Fig. 4 in Descamps et al. (2011). The solid-line contour is the shape model's silhouette scaled up with the equivalent radius inferred from radiometry, whereas the dotted line is the same shape but scaled with the radar volume-equivalent radius. See Descamps et al. and references therein for more details. The updated model of Hanus et al. (2017) based on AO also favours the radiometric diameter.

shapes have limitations, especially the left one. Reviewing these limitations in great detail is out of the scope of this document, but it is important to mention that the reconstruction of the shape is a mathematically ill-posed inverse problem that requires some assumptions and simplifications (see Ďurech et al. 2015, and references therein), and that the resolution attainable with the current state of the art is limited to about 30 milliarcseconds. This allows us to observe only the largest two hundred main-belt asteroids. As in the case of light curve interpretation (see Sec. 3), we also require a good coverage of the rotational phase and ideally several apparitions to obtain accurate and complete shape models. For instance, in cases where the resolution is not very high and the rotational coverage is not sufficient, a dent on the AO image could be ambiguously interpreted as a real dent on the object while being in reality due to a shadow. In addition, the discrepancy between the radiometric- and radar-based scales shows the potential biases we can introduce when there is a single source of "ground-truth" information available.

# 3 Convex and non-convex shapes from light curve inversion (LCI)

The irregular shapes of the asteroids combined with their rotation causes their apparent brightness in visible wavelengths to vary periodically. An example is depicted in Fig. 3, acquired from the "Interactive service for asteroid models" (ISAM) website[2] (Marciniak et al. 2012). It shows two snapshots (left) of asteroid (17) Thetis at two different apparitions (top an bottom panels) and their associated synthetic light curves (right). A light curve can be obtained observationally by measuring the brightness of the body and comparing it to photometric standard stars (absolute photometry) or other comparison stars (relative photometry; for a recent review see Santana-Ros et al. 2017).

Conversely, it is possible to infer information about the shapes and spin orientations of small bodies from their light curves, but this *inverse problem* is not so straight forward. It is mathematically ill-posed, and it requires a significant number of densely-sampled, high-quality light curves to guarantee realistic model solutions. The now classical approach to obtain *unique* convex hull approximations for bodies without atmospheres from light curve inversion (LCI) was put forward by Kaasalainen et al. (2001); Kaasalainen & Torppa (2001). It has been successfully applied on an accumulated set of sparse and dense optical light curves of several hundred targets (e.g. Ďurech et al. 2010; Marciniak et al. 2011, 2012; Hanuš et al. 2013b, 2016), and in combination with other complementary sources of information: occultations (e.g. Ďurech et al. 2011), AO data (see Sec. 2 and references therein), radar and interferometric data (Viikinkoski et al. 2015), spacecraft data (Carry et al. 2012; O'Rourke et al. 2012), and even thermal data (Müller et al. 2017). A review about the reconstruction of asteroid models based on multiple sources of data is provided by Ďurech et al. (2015). We make extensive use of –and will prospectively contribute to– the DAMIT database[3] (Ďurech et al. 2010), where both convex and non-convex (based on multi-data fits) shape models and spin vectors are provided.

The limitation of the classical inversion algorithm to provide convex hulls is challenging for objects with significant concavities and irregularities (see, for example, Fig. 5). The major difficulty is that the classical approach cannot rule out an infinite part of phase space containing non-convex models, so other sources of information, such as occultations or AO mentioned above, can greatly help in this regard.

[2] Visit http://isam.astro.amu.edu.pl and SBNAF deliverable "3.2. Predictions of shape orientations" for more information and examples of the ISAM service.

[3] http://astro.troja.mff.cuni.cz/projects/asteroids3D

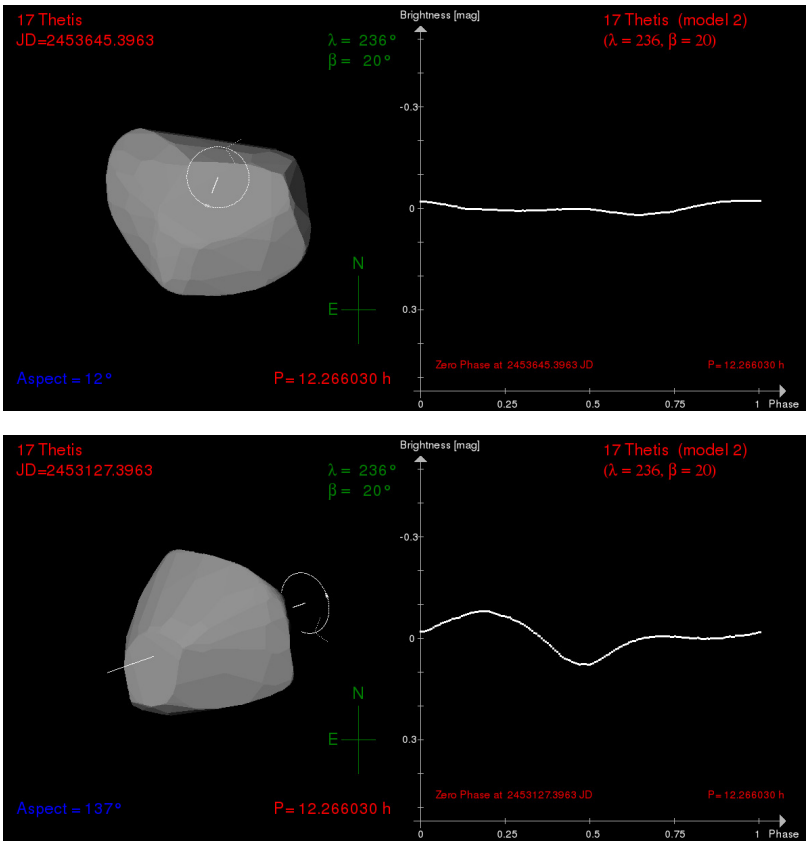


Figure 3: Two renderings (top and bottom left) of a convex shape model of asteroid (17) Thetis (Ďurech et al. 2009) and the corresponding light curves (top and bottom right). Both the irregular shape and the orientation of the spin axis determine the light curve patterns. Objects observed close to pole-on, as in the top panel, produce very shallow (low-amplitude) light curves.

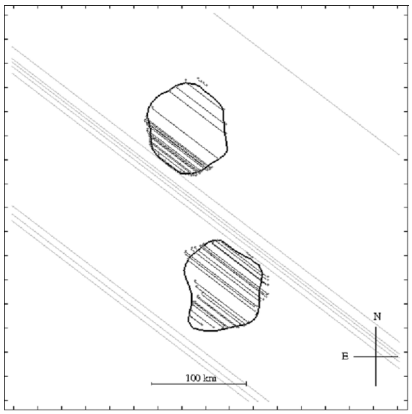


Figure 4: Silhouettes of the non-convex shape models derived with SAGE for binary asteroid (90) Antiope and the occultation chords of the 2011 event used to scale them (Bartczak et al. 2014, and references therein).

Bartczak et al. (2014) proposed the "Shaping Asteroids with Genetic Evolution" (SAGE) algorithm to derive non-convex shapes based on LCI alone. They used a genetic algorithm that starts with a spherical shape, generates random populations of shapes and spin axis orientations, and finds the best-fitting model to the data. Then, said model is used as a seed for next population in subsequent iteration, and the algorithm is stopped when shapes do not change significantly from one iteration to another.

In addition, Bartczak & Dudziński, (accepted for publication in MNRAS) have shown the capabilities of SAGE to reproduce a set of five synthetic shapes, the shape of spacecraft-visited, near-Earth asteroid (433) Eros, and the occultation chords and AO data of main-belt asteroid (9) Metis.

# 4 Summary of several published works and target information

The following items summarise the targets featured in articles accepted for publication:

- Bartczak & Dudziński (accepted) obtained non-convex shape models of (433) Eros (Sec. 4.1) and (9) Metis (Sec. 4.2) from LCI with SAGE.
- Marsset et al. (2017)(including T. G. Müller) obtained a non-convex shape for asteroid (6) Hebe based on AO and stellar occultations data using the ADAM algorithm (Sec. 4.3).
- Marciniak et al. (accepted) features two targets with occultation data (see Table 1) amenable to LCI with SAGE, namely
  - (159) Aemilia
  - (329) Svea

  Another three targets whose shape solutions are being tested with thermo-physical modelling are featured in this publication.

In addition, Butkiewicz-Bąk et al. (2017) studied a set of synthetic shape models to gain statistical insight into biases affecting period determinations in cases where not all possible light curve extrema are sampled. Although this is not related to ground-truth shapes, it will help identify potential difficulties in the reconstruction of reliable shapes for objects with ground truth data.

## 4.1 (433) Eros

Near-Earth asteroid (433) Eros was visited by the NEAR-Shoemaker spacecraft, making it an important benchmark prototype. Thomas et al. (2002) provided a stereogrammetric shape model based on tens of thousands of resolved images. We have derived a non-convex shape model for Eros using SAGE (Bartczak & Dudziński, accepted). It is interesting to compare the SAGE model with the early convex model derived from LCI (see Fig. 5, taken from Figure 5 in Torppa 2007, Ph.D. thesis[4]).

For further comparison, Table 1 contains information taken from the two entries for Eros found in the occultation-based sizes compiled in Dunham et al. (2016). Notice how the best-fitting solution to good-quality chords (the 1975 entry) leads to a circle-equivalent diameter of 10.1 km, which is considerably smaller than the 16.9 mean diameter obtained from spacecraft data by Thomas *et alia*. This shows that care must be exersised when scaling shape models based on single occultation events and how important it is to combine different sources of information.

[4] Available at http://urn.fi/URN:ISBN:978-952-10-4416-8

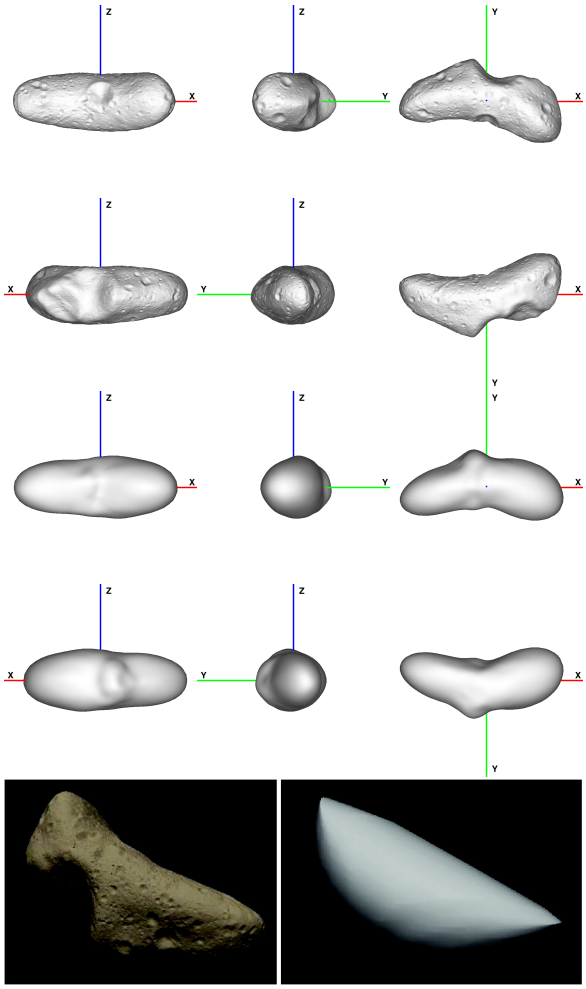

Figure 5: Top panel: Projections of the ground-truth shape model of (433) Eros (Thomas et al. 2002) and the SAGE solution (Bartczak & Dudziński, accepted). Lower panel: Rendering of the ground-truth shape (left) and the convex shape derived from LCI (digitised from Figure 5 in Torppa 2007, Ph.D thesis).

| Designation | Major axis (km) | Minor axis (km) | Equiv. diameter (km) | Quality code | Date |
|---|---|---|---|---|---|
| (6) Hebe | 240.6 | 182.0 ± 10.4 | 209.3 | 2 | 1977-03-05 |
| (6) Hebe | 207.5 ± 1.4 | — | 207.5 | 2 | 2008-02-20 |
| (9) Metis | 193.5 ± 20.7 | 117.8 ± 20.0 | 151.0 | 2 | 1989-08-06 |
| (9) Metis | 217.5 ± 8.1 | 122.3 ± 1.3 | 163.1 | 2 | 2001-09-07 |
| (9) Metis | 176.1 ± 1.0 | 161.1 ± 2.6 | 168.4 | 4 | 2008-09-12 |
| (9) Metis | 236.4 | 166.4 | 198.3 | 2 | 2008-12-29 |
| (9) Metis | 200.5 | 137.3 | 165.9 | 3 | 2012-10-08 |
| (9) Metis | 182.3 ± 1.9 | 153.1 ± 2.0 | 167.1 | 4 | 2014-03-07 |
| (130) Elektra | 216.8 ± 54.8 | — | 216.8 | 2 | 2007-11-01 |
| (130) Elektra | 247.0 | — | 247.0 | 2 | 2009-12-01 |
| (130) Elektra | 255.4 ± 6.6 | 154.5 ± 2.3 | 198.6 | 3 | 2010-02-20 |
| (130) Elektra | 292.9 | 209.4 | 247.7 | 2 | 2013-10-05 |
| (159) Aemilia | 158.8 ± 1.2 | 126.5 ± 6.6 | 141.7 | 2 | 2009-05-02 |
| (329) Svea | 83.3 ± 2.3 | 60.3 ± 1.2 | 70.9 | 3 | 2011-12-28 |
| (329) Svea | 68.9 ± 0.7 | — | 68.9 | 2 | 2013-03-07 |
| (433) Eros | 14.8 ± 0.2 | 6.9 ± 0.3 | 10.1 | 3 | 1975-01-24 |
| (433) Eros | 26.4 | 11.5 | 17.4 | 2 | 2011-12-13 |

Table 1: Major and minor axes of best-fitting ellipses to stellar occultation chords compiled by Dunham et al. (2016). A quality code of 2 indicates that a poor fit was obtained, whereas 3 and 4 mean good and excellent fits, respectively. Some quality-2 fits do not have error estimates. Empty "Minor axis" entries correspond to cases where a sphere was the best-fitting shape.

### 4.2 (9) Metis

There is a great wealth of data available for this object, which made it another ideal benchmark case for our work on the SAGE algorithm (Bartczak & Dudziński, accepted). In Fig. 6 we show Gemini and Keck AO data (Marchis et al. 2006; Drummond et al. 2012; Hanuš et al. 2013a) along with projections of shape models derived from other algorithms (convex inversion,KOALA, and ADAM) and our own SAGE shape model.

Table 1 contains six entries taken from Dunham et al.'s compilation of occultation-based sizes, three of which are labelled with quality codes 3 and 4, indicating the fits to the observations were good or excellent, respectively. The convex (Ďurech et al. 2011) and non-convex (Hanuš et al. 2013a, , based on AO+LCI) shapes available in the DAMIT database may be useful for future thermo-physical analyses. Hanus et al. (2017) provided an updated AO-based size of 168 ± 3 km that is in very good agreement with the high-quality fits to occultation chords (see Table 1).

### 4.3 (6) Hebe

There is an article in preparation with contributions from one of our members (Marsset et al.; including T. G. Müller) on the shape reconstruction of this target based on VLT/SPHERE observations. The best-fitting equivalent diameters to occultation chords (Table 1) suggest a discrepancy of ~20%

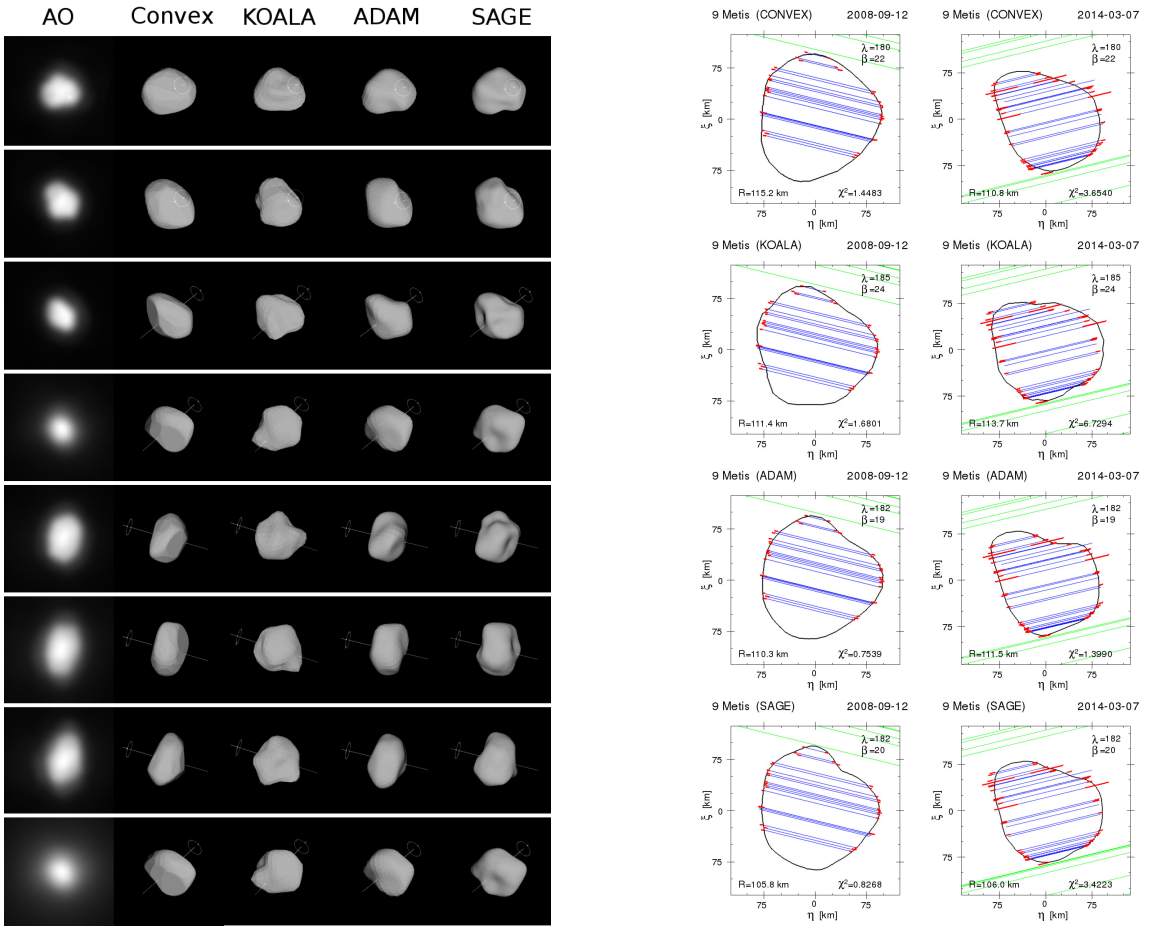


Figure 6: Comparison of shape models obtained from different algorithms with AO data (left panel) and occultations (right panel). We include convex hulls (Kaasalainen et al. 2001), KOALA (Carry 2012), ADAM (Viikinkoski et al. 2015), and SAGE (Bartczak & Dudziński) models.

with respect to previous AO-based estimates (165±21 km; Hanuš et al. 2013a). Although the quality of the fit to the occultation data is poor, the updated value of size by Marsset et al. is in good agreement.

### 4.4 (159) Aemilia and (329) Svea

Occultation-based dimensions for these two targets are given in Table 1. There is no other ground-truth source of data, but there is a considerable number of thermal IR data available, which makes these interesting targets for scientific study.

# 5 Targets featured in on-going work or planned future work

## 5.1 (21) Lutetia

We have already collected ground-truth based and AO-based shapes and rotational states for this object in deliverable D6.2, as well as important physical properties in deliverable D6.3. For our comparison purposes, the convex shape of Torppa et al. (2003) (available from DAMIT) may also be useful. Deliverable 3.2 (Figure 5) shows a plot of Lutetia's recently obtained chords (occultation event of 10 February 2017), preliminarily fitted to its KOALA model contour (Carry et al. 2012). We are also considering the usefulness of WISE 3.4 $\mu$m data, mostly dominated by reflected sunlight, in the LCI method, with the caveat that, depending on the geometry of observation, the contributions of thermal emission can be non-negligible, even at these wavelengths.

## 5.2 (25143) Itokawa

We already collected ground truth information of Itokawa in deliverable D6.3. The convex and ground-truth (Gaskell) shape models were already discussed by Müller et al. (2014b) in the context of thermo-physical modelling. As an important addition, we have obtained a (resolved) visible light curve from exposures taken from the Hayabusa spacecraft during its approach, which provide information at very atypical viewing geometries. They will be combined with literature data to obtain a non-convex shape model with SAGE, which will constitute a very complete benchmark case.

# 6 Other SBNAF targets with available ground-truth shape information

We have also compiled information on targets that already have somewhat incomplete ground truth information (partial shape coverage from fly-bys of 951 Gaspra, 253 Mathilde) or that will be observed independently of SBNAF and within the project's duration, e.g. the Hayabusa-2 target (162173) Ryugu, the OSIRIS-REx target (101955) Bennu. Also, some of the targets in the ESO large program of P.I. Pierre Vernazza (see Sec. 2) could become SBNAF targets. There are already several targets within our potential secondary calibrators list (see deliverable D4.6) for which Hanuš et al. (2016); Hanus et al. (2017) have obtained shape models based on the combination of occultation, light curve, and/or AO data. These shapes will also be collected as soon as they are made available in the DAMIT database.

Potential secondary calibrators (D4.6) and other SBNAF targets featured in Hanuš et al. (2013a) with available shapes for which no update in the DAMIT database is pending are asteroids numbered 14, 23, 37, 68, 423. Table 2 contains occultation-based sizes. A first assessment of potential secondary calibrators shape models (those presently available from the literature) is featured in deliverable D3.3 (only available to the members of the SBNAF consortium).

Finally, for different kinds of reasons, not all SBNAF targets are adequate for LCI, so they are not considered here. In some cases, for example, they are too regularly-shaped, like Ceres, or have notable albedo variegations, such as Vesta (see deliverable D6.2). These two objects are nonetheless part of our four primary calibrators because their fluxes have been extensively proven to be accurately predictable (Müller et al. 2014a). Other targets do not have a sufficiently comprehensive data

coverage and more (photometric or occultation) observations within SBNAF's time frame will not allow us to probe aspect angles of the body that have never been observed before.

| Designation | Major axis (km) | Minor axis (km) | Equiv. diameter (km) | Quality code | Date |
|---|---|---|---|---|---|
| (14) Irene | 188.0 | 135.0 | 159.3 | 2 | 1996-01-24 |
| (14) Irene | 164.0 ± 10.7 | 118.3 ± 8.6 | 139.3 | 2 | 2013-08-02 |
| (37) Fides | 89.5 ± 9.2 | — | 89.5 | 2 | 1996-08-12 |
| (37) Fides | 114.0 | — | 114.0 | 2 | 2010-09-01 |
| (68) Leto | 151.0 | 126.0 | 137.9 | 2 | 1999-05-23 |
| 423 Diotima | 221.0 | 112.0 | 157.3 | 2 | 2000-01-07 |
| 423 Diotima | 171.9 ± 4.2 | 140.7 ± 3.6 | 155.5 | 3 | 2001-03-15 |
| 423 Diotima | 172.0 | 172.0 | 172.0 | 2 | 2010-12-10 |

Table 2: Major and minor axes of best-fitting ellipses to stellar occultation chords compiled by Dunham et al. (2016). A quality code of 2 indicates that a poor fit was obtained, whereas 3 and 4 mean good and excellent fits, respectively. Some quality-2 fits do not have error estimates.

| Body | Occultation | AO | Comments |
|---|---|---|---|
| (1) Ceres | Millis et al. (1987) | Drummond et al. (1998) | *Too regular for LCI.* |
| (4) Vesta | Dunham et al. (1991) | Drummond et al. (1998) | *Too strong albedo variegation for LCI* |
| (21) Lutetia | Carry (2012) and references therein | Carry (2012) and references therein | ~50% coverage by spacecraft (Sierks et al. 2011).<br>TIR data: Herschel (95, from 70 to 500 $\mu$m), AKARI (8), IRAS (5) (Müller et al. 2014a).<br>SAGE model will be produced |
| (243) Ida | - | - | 276° covered by spacecraft (at diff. resolutions Thomas et al. 1996)<br>TIR data: AKARI (9), WISE (7).<br>*Not well sampled by optical light curves to ensure a high-quality SAGE model.* |
| (253) Mathilde | Low-quality (2015) (Dunham et al. 2016) | - | ~60% coverage by spacecraft (Thomas et al. 1999)<br>TIR data: AKARI (6), IRAS (7), Herschel (8)<br>*Non-principal axes rotator.* |
| (951) Gaspra | - | - | ~ 80% coverage by spacecraft (at diff. resolutions Thomas et al. 1994).<br>TIR data: AKARI (2), WISE (33). Two convex solutions by Hanuš et al. (2013b).<br>Good prospects for SAGE modelling. |
| (2867) Steins | - | -<br>- | Partial coverage. Spacecraft-based model has a "seam" (artefact).<br>TIR data: WISE (23), Herschel (2/4)<br>Good prospects for SAGE modelling. |
| (5535) Annefrank | - | - | Partial coverage by spacecraft<br>*No purely thermal data available* |
| (433) Eros | Two events compiled by Dunham et al. (2016) | - | Full coverage by spacecraft (see also D6.3)<br>SAGE shape produced (Bartczak & Dudziński, accepted)<br>TIR data: AKARI (5), Herschel (8) |
| (4179) Toutatis | - | - | No spacecraft-based model produced (Huang et al. 2013).<br>~50% coverage by spacecraft.<br>*Non-principal axes rotator.* |
| (25143) Itokawa | - | - | Full coverage by spacecraft.<br>TIR data: AKARI (6), IRTF (5), TIMMI2 (20) (Müller et al. 2005)<br>Good prospects for SAGE modelling. |

Table 3: Data availability of asteroids visited by spacecraft. Reasons to reject them as interesting targets for SAGE modelling are given in italics. We have included cases for which the flybys provided images with sufficient resolution, which is why (9969) Braille, (5535) Annefrank and (253) Ida I Dactyl are not considered here.

## References


Bartczak, P., Michałowski, T., Santana-Ros, T., & Dudziński, G. 2014, MNRAS, 443, 1802

Carry, B. 2012, Planet. Space Sci., 73, 98

Carry, B., Kaasalainen, M., Merline, W. J., et al. 2012, P&SS, 66, 200

Descamps, P., Marchis, F., Berthier, J., et al. 2011, Icarus, 211, 1022

Drummond, J. D., Fugate, R. Q., Christou, J. C., & Hege, E. K. 1998, Icarus, 132, 80

Drummond, J. D., Merline, W. J., Conrad, A., et al. 2012, in AAS/Division for Planetary Sciences Meeting Abstracts, Vol. 44, AAS/Division for Planetary Sciences Meeting Abstracts, 302.09

Dunham, D. W., Herald, D., Frappa, E., et al. 2016, NASA Planetary Data System, 243

Dunham, D. W., Osborn, W., Williams, G., et al. 1991, in LPI Contributions, Vol. 765, Asteroids, Comets, Meteors 1991, 54

Ďurech, J., Carry, B., Delbo, M., Kaasalainen, M., & Viikinkoski, M. 2015, Asteroid Models from Multiple Data Sources, ed. P. Michel, F. E. DeMeo, & W. F. Bottke, 183–202

Ďurech, J., Kaasalainen, M., Herald, D., et al. 2011, Icarus, 214, 652

Ďurech, J., Kaasalainen, M., Warner, B. D., et al. 2009, A&A, 493, 291

Ďurech, J., Sidorin, V., & Kaasalainen, M. 2010, A&A, 513, A46

Hanus, J., Viikinkoski, M., Marchis, F., et al. 2017, ArXiv e-prints

Hanuš, J., Marchis, F., & Ďurech, J. 2013a, Icarus, 226, 1045

Hanuš, J., Marchis, F., Viikinkoski, M., Yang, B., & Kaasalainen, M. 2017, A&A, 599, A36

Hanuš, J., Ďurech, J., Brož, M., et al. 2013b, A&A, 551, A67

Hanuš, J., Ďurech, J., Oszkiewicz, D. A., et al. 2016, A&A, 586, A108

Huang, J., Ji, J., Ye, P., et al. 2013, Scientific Reports, 3, 3411

Kaasalainen, M. & Torppa, J. 2001, Icarus, 153, 24

Kaasalainen, M., Torppa, J., & Muinonen, K. 2001, Icarus, 153, 37

Marchis, F., Kaasalainen, M., Hom, E. F. Y., et al. 2006, Icarus, 185, 39

Marciniak, A., Bartczak, P., Santana-Ros, T., et al. 2012, A&A, 545, A131

Marciniak, A., Michałowski, T., Polińska, M., et al. 2011, A&A, 529, A107

Marsset, M., Carry, B., Dumas, C., et al. 2017, A&A, 604, A64

Millis, R. L., Wasserman, L. H., Franz, O. G., et al. 1987, Icarus, 72, 507

Müller, T., Balog, Z., Nielbock, M., et al. 2014a, Experimental Astronomy, 37, 253

Müller, T. G., Hasegawa, S., & Usui, F. 2014b, PASJ, 66, 52

Müller, T. G., Sekiguchi, T., Kaasalainen, M., Abe, M., & Hasegawa, S. 2005, A&A, 443, 347

Müller, T. G., Ďurech, J., Ishiguro, M., et al. 2017, A&A, 599, A103

O'Rourke, L., Müller, T., Valtchanov, I., et al. 2012, Planet. Space Sci., 66, 192

Santana-Ros, T., Dudziński, G., & Bartczak, P. 2017, Astrophysics and Space Science Proceedings, 46, 55

Sierks, H., Lamy, P., Barbieri, C., et al. 2011, Science, 334, 487

Thomas, P. C., Belton, M. J. S., Carcich, B., et al. 1996, Icarus, 120, 20

Thomas, P. C., Joseph, J., Carcich, B., et al. 2002, Icarus, 155, 18

Thomas, P. C., Veverka, J., Bell, J. F., et al. 1999, Icarus, 140, 17

Thomas, P. C., Veverka, J., Simonelli, D., et al. 1994, Icarus, 107, 23

Torppa, J., Kaasalainen, M., Michałowski, T., et al. 2003, Icarus, 164, 346

Viikinkoski, M., Kaasalainen, M., & Durech, J. 2015, A&A, 576, A8